ARTICLE

OBC
www.rsc.org/obc

Inclusion by a fluorenyl host with volatile guests: structures, thermal stability and kinetics†

Mino R. Caira,[a] Tanya le Roex,[a] Luigi R. Nassimbeni,*[a] John A. Ripmeester[b] and Edwin Weber[c]

[a] *Department of Chemistry, University of Cape Town, Rondebosch 7701, South Africa. E-mail: xrayluigi@science.uct.ac.za; Fax: +27-21-6854580; Tel: +27-21-6502569*

[b] *Steacie Institute for Molecular Sciences, National Research Council of Canada, 100 Sussex Drive, Ottawa, Ontario, Canada K1A 0R6*

[c] *Institut für Organische Chemie, Technische Universität Bergakademie Freiberg, Leipziger Strasse 29, D-09596 Freiberg/Sachs., Germany*

Received 16th January 2004, Accepted 29th March 2004
First published as an Advance Article on the web 16th July 2004

The structures of the inclusion compounds formed by the host H = 9,9′-(biphenyl-4,4′-diyl)bis(fluoren-9-ol) with *N*,*N*-dimethylacetamide (H·2DMA and H·4DMA), 1,4-dioxane (H·3DIOX), methyl ethyl ketone (H·2MEK), as well as that of the apohost have been elucidated. The compounds were characterised by thermal analysis and solid state NMR, and the kinetics of desorption of H·4DMA, H·2DMA and H·3DIOX have been examined.

Introduction

The field of inclusion phenomena has grown dramatically in the last twenty years and clathrate compounds are an important aspect of supramolecular chemistry.[1–4] Much of the effort has been directed at the synthesis of novel host compounds[5] with specific properties and the elucidation of their structures.[6] We have concentrated our endeavours on understanding the macro-properties of such compounds, and have analysed their thermal stabilities, selectivity profiles and kinetics of enclathration and desorption.[7–9] The changes in the elastic properties of Dianin's compound brought about by guest inclusion have been analysed.[10] The control of guest selectivity by changes of pH have been demonstrated by the host binaphthol and its enclathration of substituted quinolines.[11] Host compounds containing the fluorenyl moiety have been studied extensively, as they have the capacity to enclathrate a variety of guest molecules.[12] They conform to Weber's host design specifications in that they are rigid, bulky and contain the hydroxyl moiety, which facilitates the formation of coordinato-clathrates *via* hydrogen bonding.[13] A series of such host compounds, in which the fluorenyl moieties are separated by spacers of different lengths, have been synthesised, and their crystalline inclusion compounds with a large number of guests have been reported.[14]

In this study we report on the structures of the inclusion compounds formed by the host H = 9,9′-(biphenyl-4,4′-diyl)bis(fluoren-9-ol) with *N*,*N*-dimethylacetamide (H·2DMA and H·4DMA), 1,4-dioxane (H·3DIOX), methyl ethyl ketone (H·2MEK), as well as that of the non-porous α-phase, the apohost. The compounds were characterised by Thermal Gravimetry (TG), Differential Scanning Calorimetry (DSC) and ^{13}C solid state CP/MAS NMR. The kinetics of desorption of H·4DMA, H·2DMA and H·3DIOX, were measured by a series of isothermal runs at specific temperatures, yielding estimates of the activation energies of decomposition. The atomic numbering scheme of the inclusion compounds is given in Scheme 1.

Results and discussion

Crystal structures

Suitable crystals of the apohost H were obtained by slow evaporation from a solution of H in acetonitrile. The crystals of H·4DMA were obtained by evaporating a solution of H at 25 °C, while those of H·2DMA were formed by evaporating a solution of H at 62 °C.

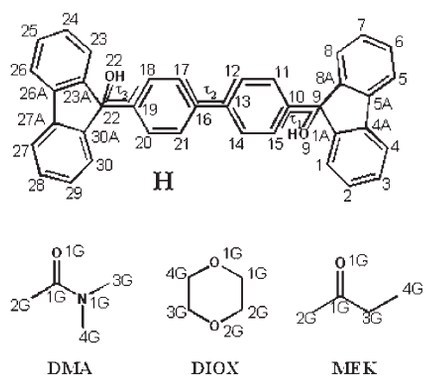

Scheme 1

In all cases the host–guest ratios were confirmed by Thermal Gravimetry (TG) and details of the crystal data, intensity data collections and refinements are given in Table 1.‡ Cell dimensions were established from the intensity data measurements on a Nonius Kappa CCD diffractometer using graphite-monochromated Mo-Kα radiation. The strategy for the data collections was evaluated using the COLLECT[15] software. For all structures, data were collected by the standard phi- and omega-scan techniques, and were scaled and reduced using DENZO-SMN[16] software. The structures were solved by direct methods using SHELX-86[17] and refined by least-squares with SHELX-97,[18] refining on F^2. The program X-Seed[19] was used as a graphical interface for structure solution and refinement using SHELX, as well as to produce the packing diagrams.

In each of the structures the positions of all non-hydrogen host atoms were obtained by direct methods and the non-hydrogen guest atoms were located in difference electron density maps. All non-hydrogen atoms were refined with anisotropic temperature factors. Hydrogen atoms were placed with geometric constraints and refined with isotropic temperature factors.

The non-porous α-phase, the apohost, crystallises in the space group $P2_1/n$ with $Z = 2$. The host molecule is located on a centre of inversion at Wyckoff position *d*. There is no hydrogen bonding between the molecules, which are packed in layers perpendicular to the *a*-axis. In a particular layer, the packing pattern approximates the plane group c2mm. Within this pattern, the molecules orientated in one direction are displaced half a unit cell length along [100], up-

† Electronic supplementary information (ESI) available: NMR spectra and assignments. See http://www.rsc.org/suppdata/ob/b4/b400721b/

‡ CCDC reference numbers 229154–229158. See http://www.rsc.org/suppdata/ob/b4/b400721b/ for crystallographic data in .cif or other electronic format.

DOI: 10.1039/b400721b

Table 1 Crystal data, experimental and refinement parameters

Compound	H	H·4DMA	H·4DMA	H·2DMA	H·3DIOX	H·2MEK
Molecular formula	$C_{38}H_{26}O_2$	$C_{38}H_{26}O_2{\cdot}4(C_4H_9NO)$	$C_{38}H_{26}O_2{\cdot}4(C_4H_9NO)$	$C_{38}H_{26}O_2{\cdot}2(C_4H_9NO)$	$C_{38}H_{26}O_2{\cdot}3(C_4H_8O_2)$	$C_{38}H_{26}O_2{\cdot}2(C_4H_8O)$
Host : guest ratio	—	1 : 4	1 : 4	1 : 2	1 : 3	1 : 2
M_r/g mol^{-1}	514.59	863.08	863.08	688.83	778.90	658.80
Crystal symmetry	Monoclinic	Triclinic	Triclinic	Triclinic	Monoclinic	Monoclinic
Space group	$P2_1/n$	$P\bar{1}$	$P\bar{1}$	$P\bar{1}$	$P2_1/c$	$P2_1/n$
a/Å	5.8002(1)	10.2961(1)	20.1219(3)	7.9629(3)	13.1096(3)	7.7993(1)
b/Å	14.4736(3)	14.9893(2)	15.1319(2)	9.0266(4)	12.8883(2)	21.9845(4)
c/Å	15.751(3)	17.8825(3)	17.3526(3)	13.5092(7)	12.0038(2)	21.0296(4)
α/°	90.00	108.255(1)	108.555(1)	77.015(2)	90.00	90.00
β/°	91.141(1)	91.524(1)	91.152(1)	83.033(2)	92.247(1)	94.552(1)
γ/°	90.00	109.284(1)	106.749(1)	84.212(2)	90.00	90.00
V/Å^3	1322.03(4)	2447.71	4759.90	936.47(7)	2026.61(7)	3594.44(11)
Z	2	2	4	1	2	4
μ(Mo-K)/mm^{-1}	0.078	0.076		0.077	0.085	0.076
Temperature (K)	298	298	113	298	173	173
Range scanned, θ(°)	1.91–27.49	1.60–27.48		1.55–25.35	1.55–27.50	1.94–26.39
Index range	h: 0–7; k: ±18; l: ±20	h: −12–13; k: ±19; l: ±23		h: ±9; k: ±10; l: −11–16	h: ±17; k: −16–15; l: ±15	h: ±9; k: −27–25; l: −26–20
No. reflections collected	5370	18802		4708	7890	17163
No. unique reflections	3027 (R_{int} = 0.0160)	11071 (R_{int} = 0.0361)		3328 (R_{int} = 0.0169)	4628 (R_{int} = 0.0221)	7322 (R_{int} = 0.0324)
No. reflections with $I > 2\sigma I$	2479	5786		2008	3355	5891
Data/restraints/parameters	3027/0/182	11071/16/577		3328/0/239	4628/0/263	7322/0/457
Final R indices ($I > 2\sigma I$)	R_1 = 0.0430	R_1 = 0.0894		R_1 = 0.0694	R_1 = 0.0468	R_1 = 0.0440
	wR_2 = 0.1123	wR_2 = 0.2508		wR_2 = 0.1723	wR_2 = 0.1071	wR_2 = 0.1027
R indices (all data)	R_1 = 0.0541	R_1 = 0.1611		R_1 = 0.1195	R_1 = 0.0729	R_1 = 0.0582
	wR_2 = 0.1198	wR_2 = 0.2990		wR_2 = 0.2034	wR_2 = 0.1191	wR_2 = 0.1106
Largest diff peak and hole (e Å^{-3})	0.230; −0.178	0.652; −0.404		0.565; −0.267	0.287; −0.202	0.218; −0.179

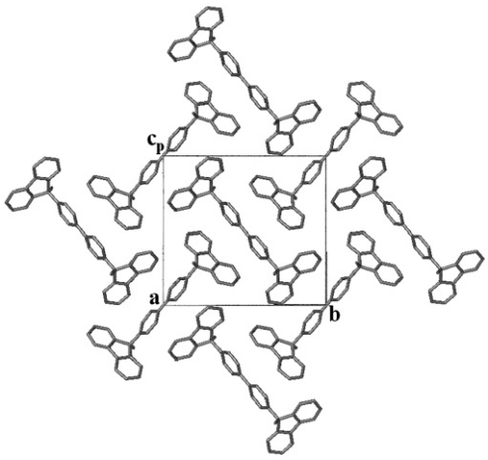

Fig. 1 Packing diagram of the apohost viewed along [100].

ward or downward from those orientated in the other direction. The structure shows a sawtooth pattern along [101]. The crystal packing viewed down the *a*-axis is shown in Fig. 1.

The structure of H·4DMA was found to undergo a phase change when cooled to 113 K. Single crystal X-ray data were collected at both 298 K and 113 K. The structure at 113 K shows an effective doubling of the *a*-axis, however this structure could not be refined to a satisfactory level and so we only report the unit cell parameters and space group for this structure. The structure of H·4DMA at 298 K crystallises in the space group $P\bar{1}$ with $Z = 2$. Due to the data being collected at 298 K, the values of the U_{eq} of the guest atoms are high. Both the host molecules and guest molecules are located in general positions. There are layers of host molecules parallel to the *ac* plane located at $y = 0.25$ and $y = 0.75$, giving rise to an open structure. The crystal packing viewed along [100] is shown in Fig. 2. Each host molecule is hydrogen bonded to two of the guest molecules *via* the hydroxyl groups with O···O distances of 2.729(3) Å and 2.756(3) Å.

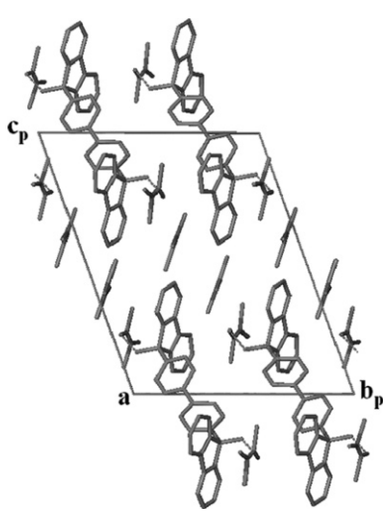

Fig. 2 Packing diagram of H·4DMA viewed along [100].

The other two guest molecules are not involved in hydrogen bonding. H·2DMA crystallises in the space group $P\bar{1}$ with one host and two guest molecules per unit cell. The host molecules are located on a centre of inversion at Wyckoff position *d* and the guest molecules are located in general positions. The host molecules pack to form channels along [−101] in which the guest molecules are located. These channels are shown in Fig. 3. The cross-sectional area of the channels is approximately 5.9 Å × 7.1 Å where the guests are located and varies only slightly from this size. The crystal packing viewed along [010] is shown in Fig. 4. Each host molecule is hydrogen bonded to two guest molecules *via* the hydroxyl groups with O···O distances of 2.747(3) Å.

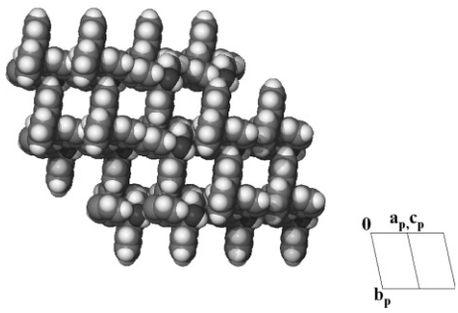

Fig. 3 View down the channels of H·2DMA along [−101] with guests omitted and host molecules represented with van der Waals radii.

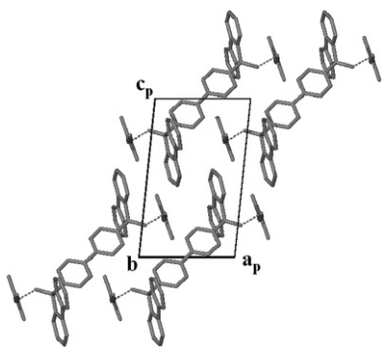

Fig. 4 Packing diagram of H·2DMA viewed along [010].

H·3DIOX crystallises in the space group $P2_1/c$, with $Z = 2$. The host molecules are again located on a centre of inversion at Wyckoff position *d*. Some of the guest molecules are located on centres of inversion at Wyckoff position *c*, while some are located in general positions. The structure is very open and the host molecules pack to form zigzagged layers perpendicular to the *a*-axis giving rise to channels along [001] in which the 1,4-dioxane guest molecules are located. These channels shift in position and also change in size along the *c*-axis, with a maximum cross-section of approximately 9.4 Å × 7.4 Å and a minimum cross-section of 7.4 Å × 4.6 Å. The crystal packing viewed down [001] is shown in Fig. 5. The guest molecules located in general positions are hydrogen bonded to the host molecule with O···O distances of 2.746(2) Å, whereas the guest molecules located on centres of inversion are not involved in hydrogen bonding.

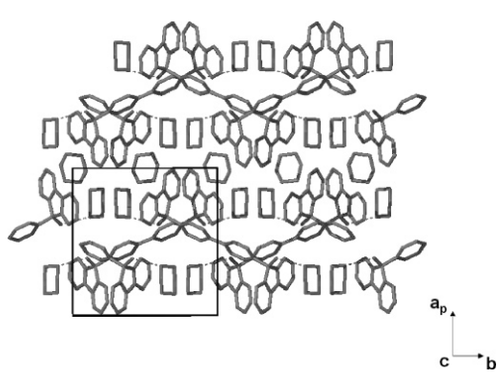

Fig. 5 Packing diagram of H·3DIOX viewed down [001].

H·2MEK crystallises in the space group $P2_1/c$ with four host and eight guest molecules per unit cell. The four host molecules are located in pairs at different centres of inversion, Wyckoff positions *b* and *d*, while the guest molecules are located in general positions. The host molecules pack to form a distorted version of the pattern seen in the structure of the apohost, resulting in undulating channels along [101] which contain the guest molecules. The channels are restricted, with maximum cross sections of 8.0 Å × 8.2 Å and minimum cross-sections of 2.0 Å × 2.4 Å. The crystal packing viewed down [010] is shown in Fig. 6. The guest molecules are hydrogen

Table 2 Torsion angles (°) describing host conformation

Compound	τ_1	τ_2	τ_3
H	−45.3(1)	0	—
H·4DMA	−23.4(4)	24.3(4)	0.8(3)
H·2DMA	10.6(4)	0	—
H·3DIOX	23.5(2)	0	—
H·2MEK	−12.5(2)	0	−29.0(2)

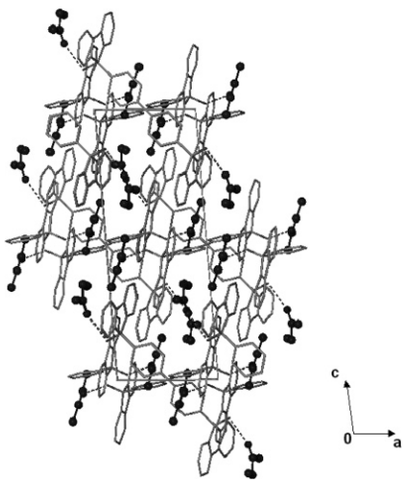

Fig. 6 Packing diagram of H·2MEK viewed down [010], with the guest molecules shown in ball-and-stick representation for clarity.

bonded to the host molecules *via* their hydroxyl groups, with O···O distances of 2.775(1) and 2.790(2) Å.

The host conformation is defined by three torsion angles, τ_1, τ_2 and τ_3, shown in Scheme 1. Table 2 compares these torsion angles of the host molecules in each of the structures.

Thermal analysis

The results of the thermal analysis are shown in Fig. 7. For both H·3DIOX and H·2MEK, the TG trace shows a one step desolvation, with a corresponding single endotherm in the DSC trace. The TG trace of H·4DMA shows a two step mass loss, with each step corresponding to the loss of two guest molecules. The DSC trace for this compound exhibits two endotherms corresponding to the two step mass loss. In each case the observed mass losses from the TG traces are in good agreement with the calculated value for that particular host : guest ratio. The final endotherm in the DSC trace of each compound corresponds to the melting of the apohost. We have noted that the difference between the onset temperature, T_{on}, and the normal boiling point of the guest, T_b, is a measure of the relative stability of an inclusion compound.[20]

The endotherm due to guest release for H·3DIOX occurs at T_{on} = 104 °C ($T_{on} - T_b$ = +3 °C). This is more stable than the dioxane inclusion compound formed with triphenylsilanol[21] ($T_{on} - T_b$ = −16 °C), but less stable than the clathrate with 10,11-dihydro-5-phenyl-5H-dibenzo[*a*,*d*]cyclo-hepten-5-ol[22]($T_{on} - T_b$ = +21 °C).[20] For H·2MEK, T_{on} = 51 °C ($T_{on} - T_b$ = −29 °C), and compares with the MEK inclusion compounds formed with 1,1,6,6-tetraphenyl-hexa-2,4-diyne-1,6-diol[22] ($T_{on} - T_b$ = −30 °C) and cholic acid[23] ($T_{on} - T_b$ = −10 °C). In the case of H·4DMA the two endotherms occur at T_{on} = 65 °C and 153 °C, corresponding to $T_{on} - T_b$ values of −100 °C and −12 °C, showing that the intermediate H·2DMA is more stable.

^{13}C solid state NMR

^{13}C solid state CP/MAS NMR was used to obtain spectra of the apohost, H·4DMA, H·2DMA, H·3DIOX and H·2MEK. The spectra were obtained at room temperature on a Tecmag 200 MHz spectrometer equipped with a Doty Scientific 7 mm CP/MAS rotor using a standard CP pulse program with fixed amplitude ^{1}H decoupling during signal acquisition. The spectra of H·4DMA, H·2DMA and

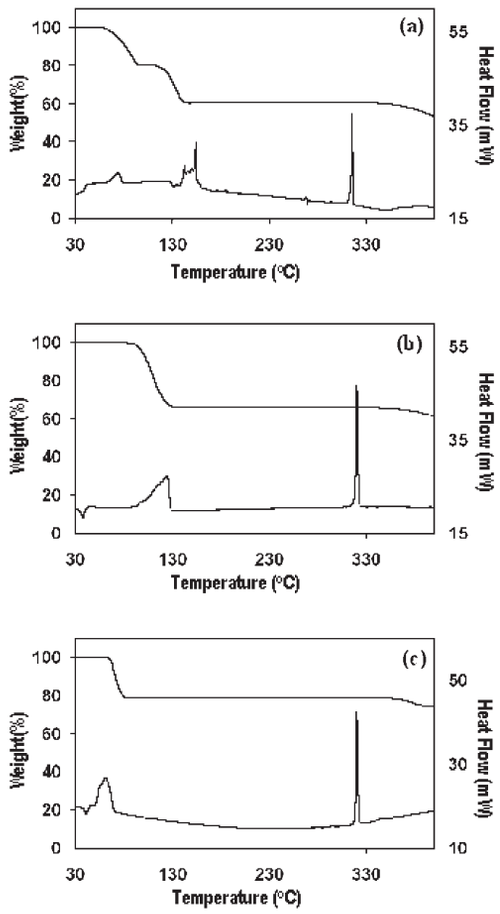

Fig. 7 TG and DSC traces of (a) H·4DMA, (b) H·3DIOX and (c) H·2MEK.

H·2MEK are shown first in each of the series given in Fig. 8(a) and (b) and Fig. 9 and the assignments of these spectra are given in Table 3. Due to the increased number of splittings in the solid state, the spectra are complicated and in each case partial assignments are given for the host resonances. The spinning sidebands in each spectrum are indicated by stars and the guest resonances are shown by arrows. The resonances in each spectrum which disappear under dipolar dephasing conditions are highlighted by a box.

Desorption of the inclusion compounds was also monitored using ^{13}C solid state CP/MAS NMR. This was carried out by running a spectrum, then removing the sample from the rotor and heating it for a period of time in the oven, then repacking and running another spectrum. This was repeated a number of times for each sample at intervals along the curve obtained by TG analysis. Fig. 8(a) shows the series of spectra obtained during the partial guest loss of H·4DMA, resulting in the H·2DMA complex. Through the series a change in the guest resonances can be seen. The host resonances also change significantly through the series, indicating a phase change which accompanies the partial guest loss.

Fig. 8(b) shows the series of spectra obtained during the guest loss from H·2DMA to form the guest-free host compound. As the sample is heated, the guest resonances decrease in size until they disappear completely. The host resonances also show a change of phase occurring simultaneously to the guest release.

Fig. 9 shows the series of spectra obtained during the release of guest from H·2MEK. Through the series the guest peaks decrease and then disappear to form guest-free host compound. Once again a simultaneous phase change is shown by the host resonances. The desorption of H·3DIOX was studied in the same manner and a similar series of spectra to that of H·2MEK was obtained.

The final spectra in each of the above series are identical, indicating that in each case the guest-free host compound formed by desorption has the same structure, which is also the same as the original host compound. These results show that in each case the

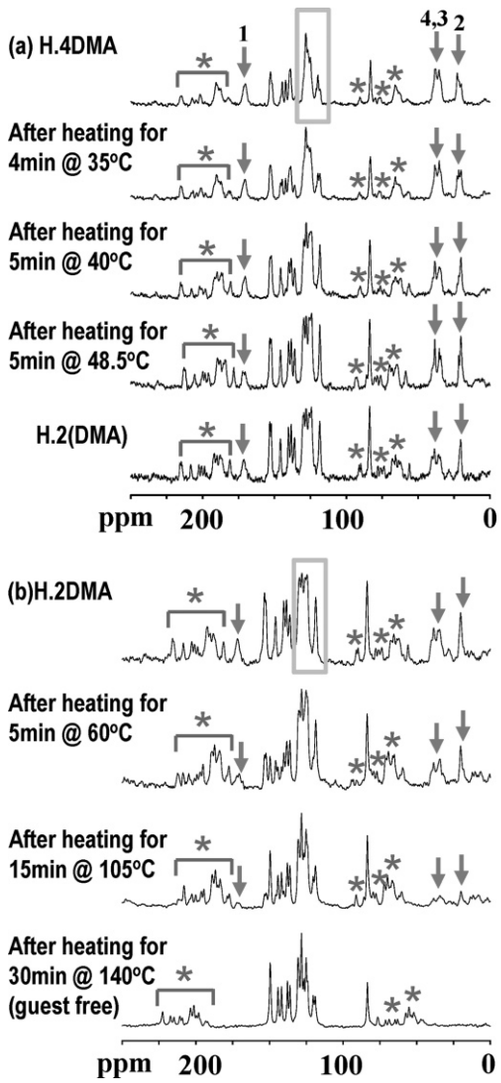

Fig. 8 ^{13}C CP/MAS spectra during desorption of (a) H·4DMA (800 scans at 15 s intervals) and (b) H·2DMA (300 scans at 10 s intervals, 5 μs 90° ^{1}H pulse, contact time = 2 ms).

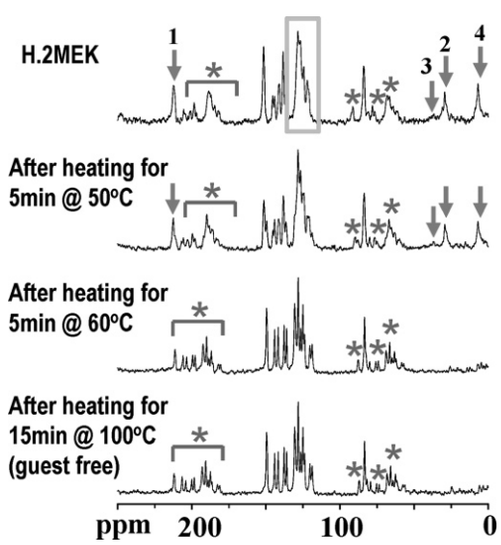

Fig. 9 ^{13}C CP/MAS spectra during desorption of H·2MEK (600 scans at 5 s intervals, 5 μs 90° ^{1}H pulse, contact time = 2 ms).

guest loss and the phase change to the structure of host alone are intimately connected and occur simultaneously.

Kinetics of desorption

The kinetics of desorption of both H·4DMA and H·3DIOX were analysed by carrying out a series of isothermal TG runs. The data were converted to extent of reaction (α) *versus* time curves. In the case of H·4DMA, the first desorption step resulting in the stable compound, H·2DMA was separated from the second desorption step by selecting appropriate temperatures for these experiments. Once the first desorption step was complete, the sample was removed and then the temperature was raised for the second desorption step and the sample replaced. Fig. 10 shows a typical example in which the mass loss *versus* time curve along with the temperature program used is shown.

Table 3 ^{13}C solid state NMR isotropic shifts and assignments of host–guest compounds[a]

Shift	Assignment C atom	
H·4DMA		
H		
152.5	1A, 8A	Q
145.1–135.2	4A, 5A, 10, 13	Q
128.7–118.4	1–8, 11, 12, 14, 15	CH
84.0	9	Q
DMA		
169.7	1	Q
38.5	4	CH_3
36.1	3	CH_3
23.8–20.5	2	CH_3
H·2DMA		
H		
154.1, 152.4	1A, 8A	Q
145.9–136.1	4A, 5A, 10, 13	Q
130.3–118.8	1–8, 11, 12, 14, 15	CH
84.4	9	Q
DMA		
171.3	1	Q
40.4	4	CH_3
35.8	3	CH_3
20.1	2	CH_3
H·2MEK		
H		
151.2	1A, 8A	Q
144.3–135.6	4A, 5A, 10, 13	Q
127.9–120.5	1–8, 11, 12, 14, 15	CH
82.8	9	Q
MEK		
219.7	1	Q
36.1	3	CH_2
27.8	2	CH_3
6.6	4	CH_3

[a] Q = quaternary carbon, Partial assignments are given where the complete assignment is not known.

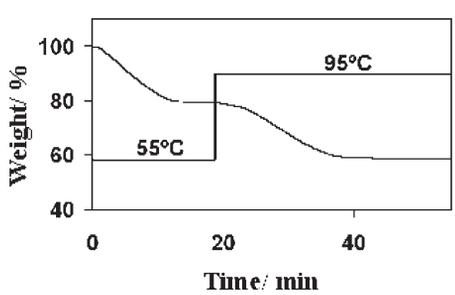

Fig. 10 Example of a set of isothermal TG experiments done on H·4DMA as well as the temperature program.

Isothermal TG experiments were carried out over the temperature range 40–65 °C at intervals of 5 °C for the first step and over the temperature range 90–110 °C also at intervals of 5 °C for the second step. The curves obtained for both the first and second desorption steps were found to fit the Prout–Tompkins equation over an α-range of 0.05–0.95. The semilogarithmic plots of ln k_{obs} *versus* 1000 K/T are shown in Fig. 11(a) and (b) and yield activation energies of 79.1 kJ mol^{-1} and 115.4 kJ mol^{-1} for the first and second steps respectively.

It is interesting to note that in inclusion compounds H·nG which desorb in two steps:

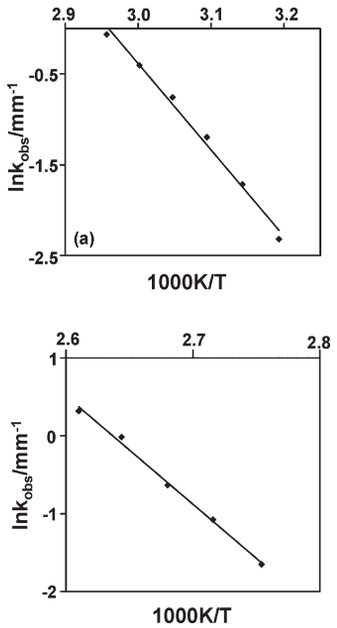

Fig. 11 Semilogarithmic plots of ln k_{obs} *vs.* 1000 K/*T* for (a) the first step and (b) the second step of the desorption of H·4DMA.

$$H\bullet nG \xrightarrow{E_1} H\bullet(n-m)G + mG\uparrow \xrightarrow{E_2} H + (n-m)G\uparrow \quad (n > m)$$

the activation energy E_1 for the first step is smaller than that of the second step E_2. This occurred with the inclusion compound formed between the host H1 = 2,2′-bis(2,7-dichloro-9-hydroxy-9-fluorenyl)biphenyl with dioxane[24] in which the desorption reaction

$$H1\cdot 3.5DIOX \rightarrow H1\cdot 1.5DIOX \rightarrow H1$$

yielded values of E_1 = 34 kJ mol^{-1} and E_2 = 111 kJ mol^{-1}. Similar results were obtained with the host binaphthol, BINAP, with dioxane, which formed the inclusion compound BINAP·3.5DIOX that decomposed to the intermediate BINAP·1.5DIOX and subsequently to the apohost BINAP. Here the activation energies measured were E_1 = 61 kJ mol^{-1} and E_2 = 86 kJ mol^{-1}. In this latter case both the starting and intermediate inclusion compounds were isolated by crystallisation at different temperatures.[25] We note that inclusion compounds with different guest : host ratios may be prepared from the same host–guest system by changing the crystallisation temperature.

The general rules linking guest/host ratios, the topologies of the ensuing compounds and crystallisation temperature have been formulated by Ibragimov,[26] and state

(i) the guest/host ratio decreases as the crystallisation temperature increases.

(ii) the topology changes from low to high temperature as intercalate → tubulate → cryptate → apohost.

Thus the compounds with high guest/host ratios generally have the more open structures. These in turn would decay easily to intermediates with lower guest/host ratios by a desorption process of low activation energy. The intermediate, with a lower guest/host ratio is then likely to be more stable and decay with a higher activation energy. This is indeed what occurred in our desorption of H·4DMA → H·2DMA → H.

The desorption of H·3DIOX takes place in a single step and isothermal TG experiments were carried out over the temperature range 70–90 °C at intervals of 5 °C. The desorption curves obtained were found to fit the first order equation over an α-range of 0.05–0.95. The semilogarithmic plot of ln k_{obs} *versus* 1000 K/*T* is shown in Fig. 12 and yields an activation energy of 95.5 kJ mol^{-1}.

Conclusion

A multiple technique approach to the study of organic inclusion compounds is useful when relating structure to macro-properties.

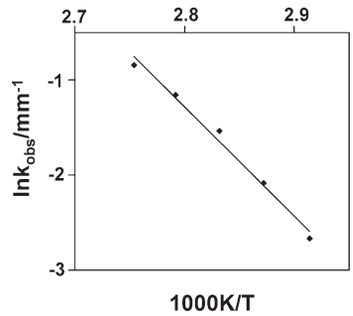

Fig. 12 Semilogarithmic plot of ln k_{obs} *vs.* 1000 K/*T* for H·3DIOX.

The packing of the host–guest systems formed between the fluorenyl host 9,9′-(biphenyl-4,4′-diyl)bis(fluoren-9-ol) and volatile guests is related to their thermal stability as measured by DSC, and solid state NMR has shown that, upon desorption, the inclusion compounds revert to the structure of the apohost. The kinetics of desorption yield activation energies which are related to the topologies of the host–guest systems.

References

1 F. Vögtle, *Supramolecular Chemistry*, Wiley, Chichester, 1991.
2 J. W. Steed and J. L. Atwood, *Supramolecular Chemistry*, Wiley, Chichester, 2000.
3 Eds. D. D. MacNicol, F. Toda and R. Bishop, *Comprehensive Supramolecular Chemistry*, vol. 6, (Crystal Engineering), Elsevier, Oxford, 1996.
4 E. Weber, in *Kirk-Othmer Encyclopedia of Chemical Technology*, Ed. J. Kroschwitz, 4th ed., Wiley, New York, 1995, vol. 14.
5 R. Bishop, *Chem. Soc. Res.*, 1996, 311.
6 Recent examples: Z. Urbanczyk-Lipkowska, K. Yoshizawa, S. Toyota and F. Toda, *CrystEngComm*, 2003, **5**, 114; K. Tanaka, T. Hiratsuka and Z. Urbanczyk-Lipkowska, *Eur. J. Org. Chem.*, 2003, 3043; F. Toda, S. Hirano, S. Toyota, M. Kato, Y. Sugio and T. Hachiya, *CrystEngComm*, 2002, **4**, 171.
7 L. R. Nassimbeni, *Acc. Chem. Res.*, 2003, **36**, 631–637.
8 L. R. Nassimbeni, *CrystEngComm*, 2003, **5**(35), 200–203.
9 O. Sumarua, J. Seidel, E. Weber, W. Seichter, B. T. Ibragimov and K. M. Beketov, *Cryst. Growth Des.*, 2003, **3**, 541.
10 J. G. Selbo, J. J. Haycraft and C. J. Eckhardt, *J. Phys. Chem. B*, 2003, **107**, 11163.
11 M. R. Caira, Y. Paul Chang, L. R. Nassimbeni and H. Su, *Org. Biomol. Chem.*, 2004, **2**, 655.
12 E. Weber, in *Comprehensive Supramolecular Chemistry*, Eds. D. D. MacNicol, F. Toda and R. Bishop, Elsevier, Oxford, 1996, vol. 6, p. 535.
13 E. Weber, in *Inclusion Compounds*, Eds. J. L. Atwood, J. E. D. Davies and D. D. MacNicol, Oxford University Press, Oxford, 1991, vol. 4, p. 188.
14 E. Weber, S. Nitsche, A. Wierig and I. Csöregh, *Eur. J. Org. Chem.*, 2002, 856–872.
15 COLLECT, Data Collection Software, Nonius, Delft, The Netherlands, 1998.
16 Z. Otwinowski and W. Minor, *Methods in Enzymology, part A: Macromolecular Crystallography*, ed. C. W. Carter Jr. and R. M. Sweet, Academic Press, New York, 1997, vol. 276, p. 307.
17 G. M. Sheldrick, in *Crystallographic Computing*, Ed. G. M. Sheldrick, C. Kruger and R. Goddard, Oxford University Press, Oxford, 1985, vol. 3, p. 175.
18 G. M. Sheldrick, SHELX-97, Program for Crystal Structure Determination, University of Göttingen, Germany, 1997.
19 L. J. Barbour, X-Seed, Graphical Interface for SHELX Program, University of Missouri-Columbia, USA, 1999.
20 M. R. Caira, L. R. Nassimbeni, M. L. Niven, W.-D. Schubert, E. Weber and N. Dörpinghaus, *J. Chem. Soc., Perkin Trans. 2*, 1990, 2129.
21 S. A. Bourne, L. Johnson, C. Marais, L. R. Nassimbeni, E. Weber, K. Skobridis and F. Toda, *J. Chem. Soc., Perkin Trans. 2*, 1991, 1707.
22 L. Johnson, L. R. Nassimbeni and F. Toda, *Acta Crystallogr., Sect. B*, 1992, **48**, 827.
23 M. R. Caira, L. R. Nassimbeni and J. L. Scott, *J. Chem. Crystallogr.*, 1994, **24**, 783.
24 M. R. Caira, A. Coetzee, L. R. Nassimbeni, E. Weber and A. Wierig, *J. Chem. Soc., Perkin Trans. 2*, 1995, 281.
25 L. R. Nassimbeni and H. Su, *J. Phys. Org. Chem.*, 2000, **13**, 368.
26 B. T. Ibragimov, *J. Incl. Phenom. Macrocyclic Chem.*, 1999, **34**, 345.